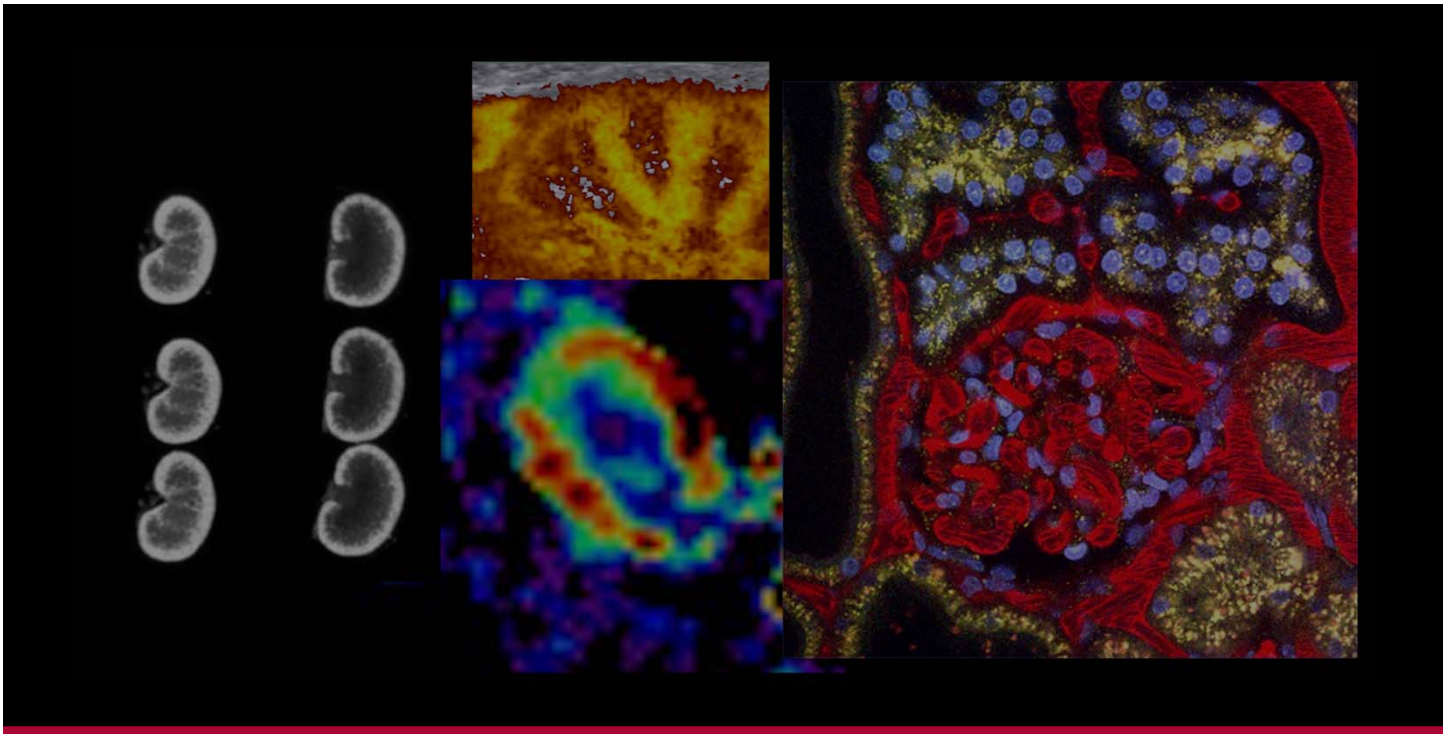

# *2016 Advances in Renal Imaging Symposium*

**November 15 & 16, 2016**

**Indiana University School of Medicine/IUPUI**

**Indianapolis, Indiana**

ISN International Society of Nephrology 1960

IUPUI

INDIANACTSI Clinical and Translational Sciences Institute

# 2016 Advances in Renal Imaging Symposium

**November 15 – 16, 2016**

**Indianapolis, Indiana**

# Table of Contents

# *2016 Advances in Renal Imaging Symposium*

IUPUI Campus Center – Lower Level

## Tuesday, November 15, 2016

***Welcome & Overview of Symposium (1:00 - 1:10 PM)***

Bruce A. Molitoris, MD – *Division of Nephrology, Department of Medicine, Indiana University School of Medicine*
Anantha Shekhar, MD, PhD, *Executive Associate Dean for Research Affairs, Indiana University School of Medicine; Director - Indiana Clinical and Translational Sciences Institute (CTSI)*

***Session 1 (1:10 - 3:10 PM)*** ***Session Topic: Need for advances in renal imaging/Potential targets for renal imaging (Chair: Bruce A. Molitoris, MD)***

- Talk 1.1 *"Role of Renal Imaging in the Kidney Precision Medicine Initiative"* (Michael F. Flessner MD, PhD – NIDDK, NIH)
- Talk 1.2 *"Assessment of Renal Fibrosis Using Magnetization Transfer MRI"* (Lilach O. Lerman, MD, PhD – Mayo Clinic)
- Talk 1.3 *"The Use of Cationic Ferritin to Quantify Glomeruli In Vivo"* (Jennifer R. Charlton, MD - University of Virginia)

***Break (3:10 - 3:30)***

***Session 2 (3:30 - 5:30 PM)*** ***Session Topic: "Advances in in vivo microscopy: extending the reach of renal imaging" (Chair: Kenneth W. Dunn, PhD)***

- Talk 2.1 *"Twice as good? Aspirational and Practical Aspects of Two-Photon Microscopy In Vivo"* (David W. Piston, PhD - Washington University in St. Louis)
- Talk 2.2 *"Label-free Optical Micro Imaging towards in vivo and in situ Assessment of Tissue Histology"* (Xingde Li, PhD - Johns Hopkins University)
- Talk 2.3 *"Intravital Fluorescence Lifetime Imaging Microscopy (FLIM): An Additional Dimension for Imaging Physiology"* (Richard N. Day, PhD - Indiana University)

***Reception/Poster session (5:30 - 6:30 PM)***

## Wednesday, November 16, 2016

***Continental Breakfast (8:00 - 8:30 AM)***

***Session 3 (8:30 - 10:30 AM)*** ***Session Topic: Advances in molecular, perfusion, structural, … renal imaging. (Co-chairs: Gary D. Hutchins, PhD & Mark R. Holland, PhD)***

- Talk 3.1 *"Renal and Urinary Tract Imaging: Classic Approaches and Future Outlook"* (Brian S. Garra, MD - Washington DC VA Medical Center & FDA DIAM)
- Talk 3.2 *"Molecular Magnetic Resonance Imaging of Renal Fibrogenesis"* (Peter Caravan, PhD – Massachusetts General Hospital and Harvard Medical School)
- Talk 3.3 *"Nanotechnologies for Diagnosis and Therapy of Acute Kidney Injury"* (Samuel A. Wickline, MD - Washington University in St. Louis)

ISN International Society of Nephrology 1960 — IUPUI — INDIANACTSI Clinical and Translational Sciences Institute

**Title: Role of Renal Imaging in the Kidney Precision Medicine Initiative**

**Author: Michael F Flessner, MD, PhD**

**Affiliation: KUH, NIDDK, NIH, Bethesda, MD**

**Abstract:**

Imaging of molecules, cells, and whole organs have an integral role in advancing medical science in the age of "Precision Medicine". At this time, nephrologists perform simple urine and blood tests to diagnose changes in kidney function and then wait, in the case of AKI, or start an ACEI or ARB, in the case of CKD. We know how to control diabetes and blood pressure, and we know that APOL1 gene mutations pose a significant risk for ESRD, but despite our best efforts, we can merely slow progression of the disease. Nephrologists rarely biopsy patients with diabetes or AKI, and there are few validated human targets to push drug development. In contrast, oncology has coupled multi-omics data with histology to tease out subgroups, pathways, and targets. This approach offers the opportunity to change Nephrology's culture and advance the study of kidney with not only phenotypic data but new histological approaches coupled with a human cell atlas and cell specific omics.

The Kidney Precision Medicine Project (KPMP) has three major components: recruitment sites, tissue interrogation sites, and a central hub to coordinate data and sample collection, digital pathology and collaboration. Recruitment sites will explore ways to safely obtain kidney tissue, and in vivo imaging will be correlated with the histopathology, the phenotype, and the genomic study of the tissue. Several speakers in this conference will address the different methods of study from elastography to MRI. Newly developed MRI tracers offer the promise of measuring the number of glomeruli or the degree of fibrosis and monitoring the response to potential therapies. The Tissue Interrogation Sites will receive the tissue from the Recruitment Sites and will use state of the art techniques and develop/optimize the "next generation" tissue interrogation methods. Some examples of these techniques will be discussed in this conference: single cell analysis using multi-color fluorescence fluctuation spectroscopy, optical coherence tomography, and use of Forster Resonance Energy Transfer Biosensors. All of these techniques have potential application in the KPMP tissue interrogation. This is an exciting time for nephrology and biomedical science.

"Advances in Renal Imaging" symposium:

**Assessment of renal fibrosis using magnetization transfer MRI**

Kai Jiang, Christopher C. Ferguson, Slobodan I. Macura, Lilach O. Lerman. Mayo Clinic, Rochester, MN.

Renal artery stenosis (RAS) decreases renal blood flow and causes a progressive loss of renal function. The stenotic kidney undergoes progressive deposition of extracellular matrix that evolves into tubulointerstitial fibrosis, an important prognostic factor in renal disease. Currently, renal biopsy is the reference method to assess renal fibrosis, but is limited by invasiveness, possible sampling error, and intra/inter-observer variability.

Several magnetic resonance imaging (MRI) techniques have been explored for noninvasive detection of renal fibrosis. Diffusion-weighted imaging is sensitive to changes in microstructure and is capable of detecting renal fibrosis, but is non-specific and largely affected by structural and functional alterations besides fibrosis. MR-elastography (MRE) measures the stiffness of tissues, which may be elevated due to fibrosis among other causes. MRE-determined medullary stiffness correlated well with medullary fibrosis in swine RAS kidneys, whereas cortical stiffness was also dependent on perfusion pressure. Alternatively, magnetization transfer imaging (MTI) can be used to evaluate the presence of macromolecules, *e.g.*, proteins, lipids, carbohydrates and nucleic acids in tissues. MTI was applied empirically for the evaluation of nephropathy, including unilateral ureteral obstruction and polycystic kidney disease.

In a recent study, we evaluated the ability of MTI to assess the progression of renal fibrosis in mice with unilateral RAS. The stenotic and contralateral kidneys were studied longitudinally *in-vivo* at baseline and 2, 4 and 6 weeks after RAS (n=10) or sham surgery (n=5). After a 16.4T MRI exam, magnetization transfer ratio (MTR) was measured as an index of fibrosis. Renal volume, perfusion, blood flow and oxygenation were also assessed with micro-MRI. Fibrosis was subsequently measured *ex-vivo* by histology and hydroxyproline assay.

In the stenotic kidney, we found that the median MTR showed progressive increases from baseline to 6 weeks in the cortex by (+13.7%) and medulla (+21.3%), which were accompanied by a progressive loss in renal volume, perfusion, blood flow, and oxygenation. The 6-week MTR map showed good correlation with fibrosis measured *ex-vivo* with trichrome staining, Sirius red staining, and the hydroxyproline assay).

Therefore, MTI successfully measured and longitudinally monitored the progression of renal fibrosis in mice with unilateral RAS. Future studies are needed to determine its sensitivity and applicability in 3T MRI.

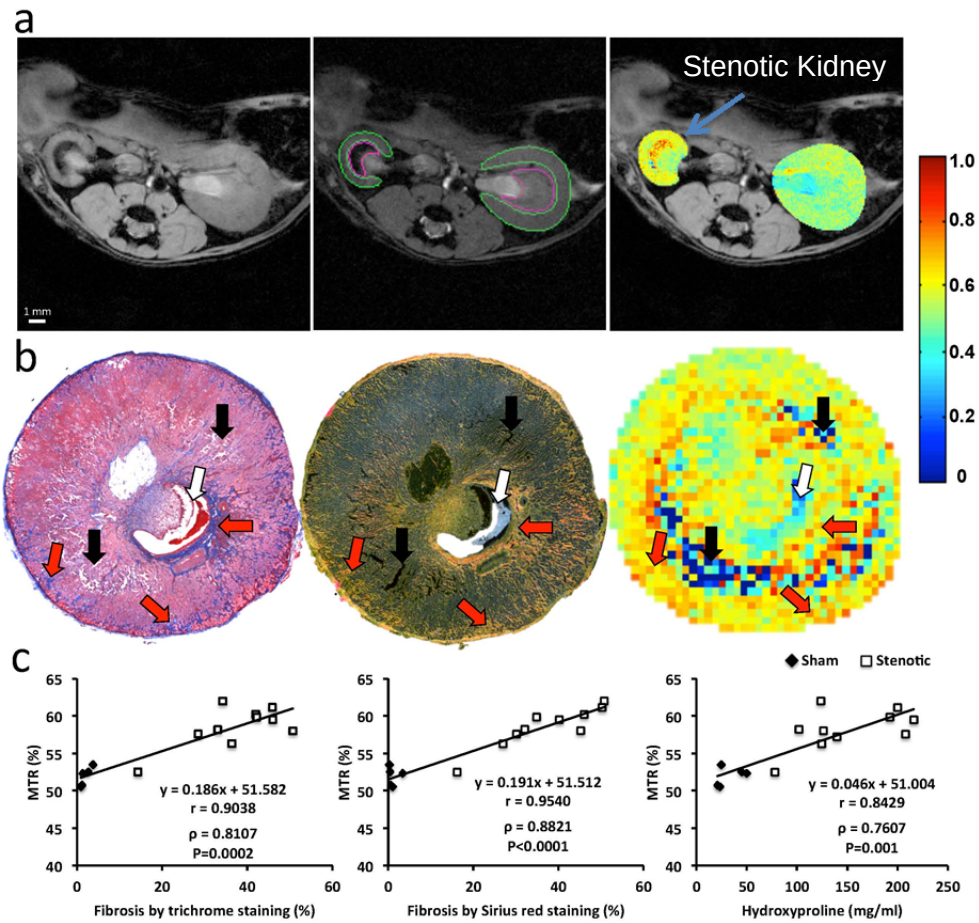


**Figure:** Renal fibrosis in mice by *in-vivo* MTI and *ex-vivo* histology or hydroxyproline assay. **(a)** MRI image without MT pulses (left), MT-weighted image with the manually traced ROIs in the cortex and medulla (middle) and calculated MTR maps overlapped with the baseline image (right). **(b)** Trichrome staining (left), Sirius red staining under polarized light (middle) (x 10), and corresponding MTR map (right) of a stenotic kidney at 6 weeks of RAS. Areas representing fibrosis, necrosis, and pelvis are marked by red, black, and white arrows, respectively. **(c)** Spearman's rank correlation of fibrosis quantified from *ex-vivo* trichrome staining (left), Sirius red staining (middle) or hydroxyproline assay (right) and *in-vivo* MTR.

**The use of cationic ferritin to quantify glomeruli *in vivo***

Jennifer R Charlton[1], Edwin J Baldelomar[2], Teresa Wu[3], Kevin M Bennett[4]

*[1]University of Virginia, Charlottesville, VA[1]; University of Hawai'i, Manoa, Department of Physics and Astronomy[2] and Biology[4]; Arizona State University Tempe, AZ*

The progression of chronic kidney disease (CKD) is insidious and often silent. Abnormal clinical diagnostic testing may indicate a state of nephron deficiency with *permanent and extensive* renal damage. The most clinically relevant biomarker for renal disease progression, glomerular filtration rate (GFR), has poor sensitivity and lacks predictive value due to the kidney's significant adaptive mechanisms that mask a reduced complement of functioning nephrons. The late manifestations of CKD and absence of early diagnostic tools to detect patients *at risk* of developing CKD have contributed to the inability to effectively halt the progression of this disease. The long-term goal of our team is to identify patients at risk for CKD to slow or halt the progression of this deadly and morbid condition. To accomplish our long-term goal, it is critical to develop the tools to acquire nephron number in a safe, noninvasive, and repeatable manner, translatable to patient care.

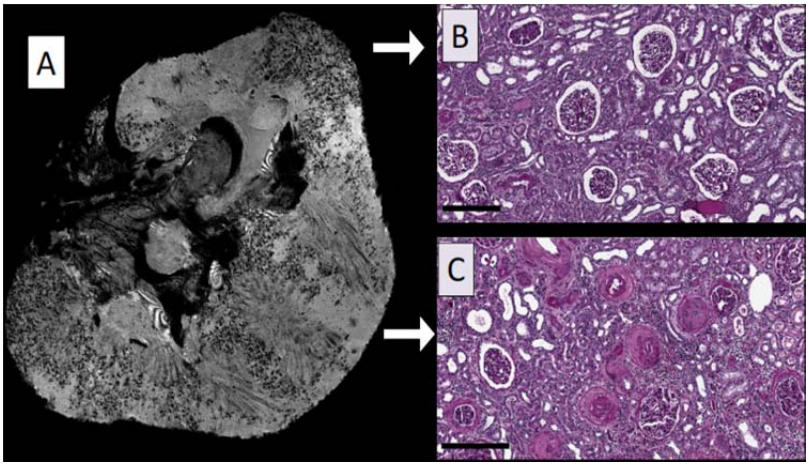


**Figure 1. CFE-MRI is used to measure glomerular morphology in human kidney *ex vivo*[4] .** (A) MR image of the kidney demonstrating large patchy regions of cortex lacking CF-labeled glomeruli. (B) The regions of cortex with CF-labeling showed mild sclerosis on histologic examination, but (C) the cortical areas that lacked CF reveal severe sclerosis of glomeruli and arterioles. The significant proportion of renal damage may be unappreciated by histologic assessments and the CFE-MRI changes precede renal functional changes.

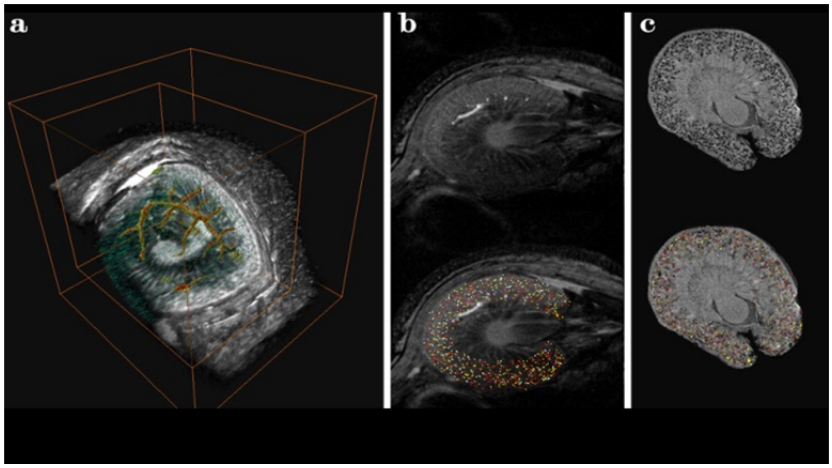


**Figure 2: CFE MRI detects glomerular morphology *in vivo* in rats:** a) 3D reconstruction of the MRI dataset showing CF-labeled glomeruli in the rat kidney *in vivo*. B) Glomeruli are segmented in 3D and c) Glomeruli are measured and counted in the images. Colored dots are individual, CF-labeled glomeruli in 2d slices from the 3D MRI dataset. The *in vivo* and *ex vivo* measurements of $N_{glom}$ and $V_{glom}$ are not different.

We have developed the technique of cationic ferritin enhanced-MRI (CFE-MRI) to detect and measure the size of individual perfused glomeruli of mice in 3D MRI[1] . CF binds to the GBM after intravenous injection and is visible in MRI as hypointense spots in labeled glomeruli of the cortex (Figure 1a)[2,3] . Without CF, glomeruli are not visible by MRI, regardless of the magnet field strength. While the number ($N_{glom}$) and volume ($V_{glom}$) measured by CFE-MRI are comparable to average values obtained using stereologic techniques, additional information gained from CFE-MRI includes intra-renal distribution of $V_{glom}$, integration of kidney compartments with 3D spatial resolution and a measure of GBM integrity and glomerular functionality. CFE-MRI has been extensively validated in healthy animals and human kidneys unsuitable for organ donation[1,3-5] . We showed that CFE-MRI can detect glomerular pathology in human kidneys prior to a change in renal function. These changes would not have been captured in histologic assessments from a biopsy (Figure 1). Our laboratories have continued to pushexpanded our ability to detect and measure glomeruli using CFE-MRI and now can identify of ALL perfused glomeruli in the kidney providing a unique view of total nephron endowment (Figure 2) and renal microstructure, both *in vivo* and *ex vivo.* Further work is required to determine how glomerular microstructure changes in disease and during disease progression. Imaging individual nephrons of the entire kidney provides a new avenue to explore the complex temporal and spatial relationships during the development of CKD.

**References:**

1. Baldelomar EJ, Charlton JR, Beeman SC, Cullen-McEwen LA, Pearl VM, Bertram JF, et al. Phenotyping by magnetic resonance imaging nondestructively measures glomerular number and volume distribution in mice with and without nephron reduction. Kidney International In press;.

2. Bennett KM, Zhou H, Sumner JP, Dodd SJ, Bouraoud N, Doi K, et al. MRI of the basement membrane using charged nanoparticles as contrast agents. Magn.Reson.Med. 2008;**60**:564-74.

3. Beeman SC, Zhang M, Gubhaju L, Wu T, Bertram JF, Frakes DH, et al. Measuring glomerular number and size in perfused kidneys using MRI. Am.J.Physiol.Renal Physiol. 2011;**300**:F1454-7.

4. Beeman SC, Cullen-McEwen LA, Puelles VG, Zhang M, Wu T, Baldelomar EJ, et al. MRI-based glomerular morphology and pathology in whole human kidneys. Am.J.Physiol.Renal Physiol. 2014;**306**:F1381-90.

5. Heilmann M, Neudecker S, Wolf I, Gubhaju L, Sticht C, Schock-Kusch D, et al. Quantification of glomerular number and size distribution in normal rat kidneys using magnetic resonance imaging. Nephrol.Dial.Transplant. 2012;**27**:100-7.

**Twice as good? Aspirational and Practical Aspects of Two-Photon Microscopy in Vivo**

David W. Piston, Ph.D.
Department of Cell Biology & Physiology
Washington University School of Medicine

Two-photon excitation microscopy provides attractive features, especially for optical sectioning deep into intact tissues or whole animals. The advantages of two-photon microscopy over linear optical sectioning techniques, such as confocal microscopy, are greater imaging depths and reduced overall photo-toxicity. Since two-photon microscopy enables dynamic cellular measurements, the extra depth penetration opens up a broad range of experiments that rely on non-invasive intra-vital imaging of cellular and sub-cellular processes. While two-photon microscopy provides the capability to perform quantitative imaging in tissues at depths well beyond those that can be reached with confocal microscopy, inherent difficulties with the non-linear optics underlying two-photon microscopy limit its main usefulness to deep-tissue imaging and a few other specialized applications. These photophysical limitations can also affect the interpretation of in vivo data, especially in situations where tissue autofluorescence is significant.

Imaging of anything thicker than a monolayer cell culture is limited by out of focus background, which can be overcome by using an optical sectioning approach, such as confocal microscopy. However, imaging live samples with confocal microscopy can create deleterious effects in the sample, in particular due to photobleaching of the probes and the phototoxicity of the excitation light. The physics underlying two-photon microscopy allows much deeper imaging with two-photon microscopy since it is much less susceptible to degradation by out-of-focus absorption and scattering. A good rule of thumb is that two-photon microscopy can provide useful image data about 6 times deeper into tissue than can confocal microscopy.

While two-photon microscopy was initially demonstrated over 25 years ago [1], for the first ~15 years, its use was limited to specialist laboratories due to the expertise needed to control the sophisticated ultra-fast laser technology required for two-photon microscopy. Nowadays, reliable 'turn-key' laser systems have been developed, allowing a hands-off approach to two-photon microscopy and rendering it as easy to drive as commercial confocal microscopes. This has allowed two-photon microscopy to transition from a novelty of the laser laboratory into a useful tool in a true biological research setting, where investigators can concentrate on studying the biological question at hand without worrying about aligning, operating, and maintaining the microscope system. Beyond the instrumentation advances, though, greater understanding of two-photon microscopy and its advantages has allowed this technique to be effectively utilized in biological research.

This talk will cover the basics of two-photon microscopy and how the underlying photophysics leads to both its advantages and limitations. To take full advantage of its strengths, the instrumentation design needs to be optimized for two-photon microscopy, and the practical aspects of two-photon photophysics and image formation need to be understood. Once these hurdles are overcome, the results can be stunning. Some recent examples of two-photon microscopy will be presented to highlight the wide range of physiological studies not only in the imaging of the kidney, but also in neuroscience, developmental biology, immunology, cancer and endocrinology.

# Label-free Optical Micro Imaging towards *in vivo* and *in situ* Assessment of Tissue Histology

*Wenxuan Liang, Scott W. Yuan, Jessica Mavadia-Shukla, Ang Li, and Xingde Li*

*Department of Biomedical Engineering, Johns Hopkins University School of Medicine, Baltimore, MD 21205 USA*

Recent years have witnessed rapid development of high-resolution optical imaging technologies such as optical coherence tomography (OCT) and multiphoton microscopy. These technologies have shown significant potential to be translated to clinical practice for imaging tissue microanatomies *in vivo* at a resolution approaching or at standard histopathology but without the need for tissue removal or processing. Thus they can function as a form of noninvasive "optical histology", which can potentially address various unmet clinical needs in early disease detection, guidance of surgical intervention, and assessment of treatment outcome. By taking advantages of some intrinsic fluorophores such as NADH and FAD, in vivo functional histology of biological tissues becomes possible. This presentation will briefly go over the evolution of these technologies and then focus on our recent advances in ultracompact endomicroscopy technologies, which literally miniaturize a bench-top scanning laser microscope down to a flexible fiber-optic scanning probe of an ~1-2 mm diameter. As one of the most recent technological developments, such a technology enables us to put a "microscope" inside an animal or human body. The physics principles, engineering challenges, (big) data and image processing challenges, and potential solutions will be briefly discussed, including the development of advanced lasers, MEMS technology, special optical fiber, ultracompact and high-performance micro optics, speckle noise reduction, image segmentation and optical staining techniques. Representative applications of these high-resolution technologies will be presented, including cancer detection, airway physiology assessment, and intra-operative guidance for neurosurgery. Potential applications for functional assessment of kidney microtubules *in vivo* and in a label-free fashion will also be presented. Other potential applications of these biophotonics imaging tools for basic research will also be discussed.

# Intravital fluorescence lifetime imaging microscopy (FLIM): an additional dimension for imaging physiology

Takashi Hato[1], Seth Winfree[1], Ruben Sandoval[1], Bruce Molitoris[1], Kenneth Dunn[1], Pierre Dagher[1] and Richard Day[2]

[1]Departments of Medicine and [2]Cellular and Integrative Physiology, Indiana University School of Medicine, Indianapolis, Indiana.

The use of two-photon laser-scanning microscopy (TPLSM) to monitor probe or auto-fluorescence signals from the tissues of living animals is of particular interest to many laboratories because it allows real-time detection of specific cellular events in their natural environment. The fluorescence signals acquired during imaging are typically separated into distinct spectral channels for analysis. There is, however, another dimension that can be captured by TPLSM – the fluorescence lifetime of the emission signals – that is often ignored in the analysis. Fluorescence lifetime is the average time that a molecule spends in the excited state before returning to the ground state through the emission of a photon. The fluorescence lifetime is an intrinsic property of a fluorophore and carries information about events that affect the excited-state. The lifetime information captured by TPLSM is visualized using phasor plots, which are a simple geometric representation of the frequency characteristics of the emission signal from each image pixel. The phasor transformation allows the rapid determination of the lifetimes of fluorescence signals emanating from tissues, and does not require any *a priori* knowledge of the fluorescent species. In the live animal, tissue auto-fluorescence arises principally from several biologically important metabolites, including the flavoproteins (FAD) and the reduced form of nicotinamide adenine dinucleotide (NADH). The phasor analysis of these auto-fluorescence signals can be used to generate “fingerprints” that identify the unique metabolic states of different cell-types within a tissue, providing a label-free imaging tool to study metabolism *in vivo*. Here, we will describe how the combination of intravital TPLSM and frequency domain FLIM is used to map cell-specific metabolic signatures in the kidney of live animals. The phasor analysis of the FLIM images enables a bias-free approach to characterize and monitor metabolism *in vivo* and offers the unique opportunity to uncover dynamic metabolic changes in living animals with subcellular resolution.

# Renal and Urinary Tract Imaging: Classic Approaches and Future Outlook

Brian S Garra, M.D.
Washington DC VA Medical Center
and
Division of Imaging, Diagnostics and Software Reliability, CDRH, FDA

Renal and Urinary Collecting System Imaging, once focused on the challenge of renal mass diagnosis, has evolved into more of a detection and patient management tool. With the advent of mildly invasive treatments of renal cancer, the need to reliably make a preoperative diagnosis has diminished since treatment often no longer involves a major operation. Even as the need for "perfect" diagnostic tools has decreased, diagnostic capabilities of existing tools have increased.

Diagnostic modalities used for renal evaluation include: plain radiography and radiographic urography, sonography (US), computed tomography (CT), magnetic resonance imaging (MRI), Radionuclide Scanning (NM), Renal Arteriography, and retrograde pyelography. Plain radiography is insensitive for most types of renal pathology and is currently used only to follow renal and ureteral calculi if they are visible on the examination. Radiographic urography, also known as excretory urography and intravenous pyelography (IVP), involves taking multiple radiographs at several times following injection of water soluble contrast material intravenously. It is useful for evaluation of the overall anatomy of the kidneys and collecting systems and especially for delineating the extent and severity of a collecting system obstruction. Because of its limited ability to delineate and detect small solid or cystic masses of the kidneys or bladder, the method has been largely replaced by CT Urography in which CT takes the place of radiography for imaging the kidneys and collecting systems. Ultrasonography detects and characterizes renal and bladder masses well and is useful for measurement of renal size and cortical thickness in chronic renal disease. It is especially useful for detection of obstruction of the urinary tract and can reliably detect stenosis of the renal arteries. Image quality degrades considerably in larger patients.

CT provides similar information to that of ultrasound but is less operator dependent and is not degraded by patient size. Because it is typically performed using intravenous contrast, it can also provide information on kidney function and can characterize the vascularity of renal masses. It is the most sensitive method for detection renal stones. MRI provides anatomic information similar to that of US and CT but provides more information about possible masses than CT when IV contrast cannot be used. It is sensitive to motion artifacts due to patient movement and bowel movement so often produces less useful images that CT. It cannot reliably detect renal calcifications or calculi. Radionuclide scanning is primarily useful for evaluation of renal function and degree of renal perfusion. It is by far the most reliable method for early detection of backflow (vesico-ureteral reflux) from the bladder into the ureters and kidney. Renal arteriography is the gold standard for detection and grading of narrowing of the renal arteries and also may be useful for characterization of renal mass vascularity – vessel morphology. Retrograde pyelography provides the most detailed evaluation of the urinary collecting system and can be used when renal function is poor.

US and CT have become the primary imaging modalities because in combination they reliably detect and characterize most anatomic abnormalities and can be used to guide biopsies and direct various treatments for obstruction and for masses. With the advent of contrast enhanced ultrasound (CEUS), US may supplant CT in thinner patients, in patients with poor kidney function or with contrast allergy for mass detection, mass characterization and perhaps in evaluation of renal perfusion. Volumetric quantification of kidney size using both CT and US will further improve monitoring of progression of chronic renal disease. Improvements in volumetric perfusion estimation using CT, US Doppler, and CEUS may allow CT and US to supplant NM for renal perfusion/function evaluation. New forms of quantitative US backscatter may also detect microscopic changes in kidney structure that can be used to monitor diffuse renal disease and early diabetic nephropathy. Finally, CEUS and CT using iterative reconstruction may allow more complete renal evaluation without the risks of IV contrast injection. Taken together, these advances will result in gradual but important improvements in imaging for diagnosis and monitoring of all forms of renal disease.

**Molecular magnetic resonance imaging of renal fibrogenesis**

Philip Waghorn[1], Iris Chen[1], Nicholas Rotile[1], Lan Wei[2], Robert Colvin[3], Bryan Fuchs[2], Peter Caravan[1].

[1.]MGH/HTS A. A. Martinos Center for Biomedical Imaging, Massachusetts General Hospital and Harvard Medical School.
[2.]Division of Surgery, Massachusetts General Hospital.
[3] Department of Pathology, Massachusetts General Hospital.

Objective:
Current noninvasive methods to detect and stage renal fibrosis are limited and there are no methods to distinguish active disease (fibrogenesis) from stable scar. The objective of this work was to develop a molecular magnetic resonance (MR) imaging probe to image fibrogenesis. During active fibrogenesis, lysyl oxidase (LOX) enzymes catalyze the oxidation of collagen lysine residues to form allysine, which enable collagen crosslinking. Quantification of allysine content would thus provide a means to determine the extent of disease activity. We report the use of 'GdOA' a novel gadolinium based MR probe designed to target allysine for non-invasive imaging of renal fibrogenesis.

Methods:
GdOA was synthesized and its interaction with allysine characterized. Two cohorts of mice were studied: Group A) sham-treated, and Group B) a nephrotoxic nephritis (NTN) model. For the NTN group '129' mice were dosed at day 0 with 250 µg Sheep IgG and then with 125 µL sheep anti-rat GBM serum at day 5. Baseline MR kidney images were acquired at day 17. Animals were then injected with GdOA and imaged again at 24h post GdOA injection. Animals were co-injected with EuDOTA as a non-binding control probe. Following MR imaging, kidneys were harvested and assessed for hydroxyproline content, Gd content in tissue and for histology.

Results:
The NTN model resulted in diffuse tubular injury (30-60%) with intratubular casts and fibrosis as indicated by trichrome staining and collagen III immunostaining. Renal hydroxyproline content was 65% higher in NTN animals compared to sham animals ($p<0.001$) Administration of GdOA resulted in a 5.7 fold increase in the change in relaxation rate, $\Delta R1$, in the NTN group compared to sham mice ($p<0.047$), correlating with increased GdOA uptake in fibrotic kidney. Ex vivo quantification of Gd revealed a 6.5 fold increase in Gd content in the NTN mice compared to sham mice ($p<0.001$). GdOA kidney uptake in NTN mice was much higher than the non-targeted control EuDOTA but there was little difference between the compounds in the sham group. $\Delta R1$ showed strong correlations with hydroxyproline ($r = 0.92$) and Gd content in tissue ($r = 0.84$).

Conclusion:
Imaging renal fibrosis with GdOA has shown strong correlation between MR signal and the extent of disease as measured by tissue content of collagen and total Gd content in tissue. GdOA may be a useful molecular probe for staging renal fibrosis and fibrogenesis.

# Nanotechnologies for Diagnosis and Therapy of Acute Kidney Injury

Samuel A. Wickline, M.D., Junjie Chen, D.Sc.
Washington University School of Medicine, St Louis, MO.

Rationale: Interest is keen for the pursuit of methods for quantifying structural and functional disruption in progressive chronic kidney disease and acute injury that might improve the sensitivity, specificity, and time in which renal injury is diagnosed, and facilitate risk stratification and/or provide prognostic information including prediction of recovery of renal function. Furthermore, novel therapeutic strategies are needed to meet the medical need for both safe and effective preventative and post-injury applications in AKI.

Imaging: Multinuclear $^{1}H/^{19}F$ MRI coupled with perfluorocarbon nanoparticle (PFC NP) contrast agents provides a noninvasive quantitative readout of kidney hypoperfusion and tissue injury (**Figure 1**). PFC NP are a class of clinically approved vehicles with no apparent toxic effect on the kidney. As a blood-pool agent, the linear relationship between the $^{19}F$ signal intensity and PFC NP concentration enables a direct measurement of blood volume in tissues. In addition, the relationship between the $^{19}F$ relaxation time (R1 = 1/T1 ) of PFC NP and dissolved $O_2$, which alters $^{19}F$ relaxation linearly according to $pO_2$, can be utilized for in vivo assessment of $pO_2$ in blood and tissue. Finally, functionalized PFC NP carrying selected targeting ligands that can bind to and report inflammatory markers (e.g. VCAM-1) may allow early detection of inflammatory kidney diseases.

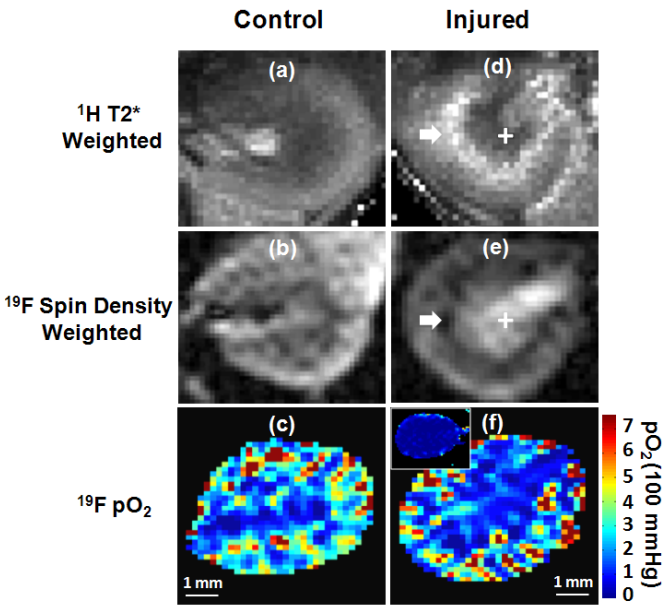


**Figure 1 MRI methods for quantifying ischemic kidney injury.** In vivo hyperoxic $^{1}H$ T2*-weighted image, $^{19}F$ spin density weighted (blood volume) image (11.7T) and $pO_2$ map in the left control (**a-c**) and right injured (**d-f**) kidneys in one mouse at 24 hr post 60 min unilateral warm ischemia. The insert in **f** shows $^{19}F$ MRI detected $pO_2$ map of another mouse kidney *during* acute ischemia: note marked global hypoxia (all blue). White arrow (**e**): injured CM junction; white cross: PFC

Therapy: We have developed and tested antithrombin nanoparticles for inhibition of microvascular thrombosis in ischemia-reperfusion injury (IRI). We designed PPACK (phenylalanine-proline-arginine-**c**hloromethyl-ketone) loaded PFC NP function as an in vivo anti-thrombin agent that effectively inhibits arterial thrombosis and platelet deposition in mice. In AKI, PPACK PFC NP effectively inhibit microvascular coagulation in mice (**Figure 2**). Mice were pre-treated (30 min) with 1ml/kg PPACK NPs or plain NP before unilateral IRI. At 3 hours after reperfusion, $^{19}F$ MRI registered higher concentrations of trapped NP in IRI kidneys than that in contralateral uninjured kidneys of the same mice, suggesting a reduction of intrarenal coagulation. To our knowledge, this is the first investigation of nanoparticle-facilitated anti-thrombotic therapy for AKI, where the effect is *directly quantifiable by imaging.*

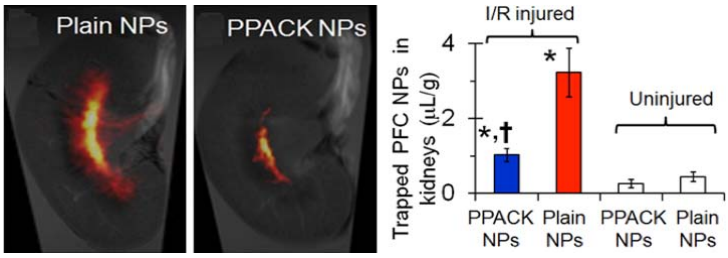


**Figure 2 Acute Kidney Injury Model: PPACK PFC NPs Inhibit Coagulation and Microangiopathy in AKI.** Left: Ex vivo $^{19}F$ MRI of kidney coregistered with $^{1}H$ anatomic image. Right: Ex vivo $^{19}F$ quantification of trapped PFC NP due to coagulation

# *2016 Advances in Renal Imaging Symposium*

## POSTER SESSION

Tuesday, November 15, 2016; 5:30 – 6:30 PM

| Poster | Title |
|---|---|
| **1** | *"Indiana Consortium for Innovation in Biomedical Imaging".* Gary D. Hutchins and Mark R. Holland; Indiana University-Purdue University Indianapolis & Indiana University School of Medicine |
| **2** | *"Research Center for Quantitative Renal Imaging".* Bruce A. Molitoris, Gary D. Hutchins, and Mark R. Holland, Indiana University-Purdue University Indianapolis & Indiana University School of Medicine |
| **3** | *"Indiana Center for Biological Microscopy"*. Kenneth Dunn, Malgorzata Kamocka, Seth Winfree, Bruce Molitoris; Indiana University School of Medicine |
| **4** | "*The 3D Bioprinting Core at IUSM/IUPUI"*. Lester J. Smith, & Nicanor I. Moldovan; Indiana University-Purdue University Indianapolis & Indiana University School of Medicine |
| **5** | *"Image-based Computational Assessment for Severity of Renal Artery Stenosis".* Huidan (Whitney) Yu[1,2], Anurag Deb[1], Avinash Mumbaraddi[1], Alan P. Sawchuk[2], Raghunandan Motaganahalli[2], Michael C. Dalsing[2]; [1]Indiana University-Purdue University, Indianapolis; [2]Indiana University School of Medicine |
| **6** | *"The Complex Hemodynamics in Aortorenal Vessel System".* Alan P. Sawchuk[2], Huidan (Whitney) Yu[1,2], Michael C. Dalsing[2]; [1]Indiana University-Purdue University, Indianapolis; [2]Indiana University School of Medicine |
| **7** | *"High Frequency Ultrasound of In Vivo Murine Renal Artery and Vein Blood Flow."* Frederick Damen[1], Arvin Soepriatna[1], Shelby Abrams[1], Amy Bogucki[1], Ron Korstanje[2], Craig J. Goergen[1]; [1]Purdue University; [2]The Jackson Laboratory, Bar Harbor, ME |
| **8** | *"Detection of Lipid-Laden Plaques by Intravascular Ultrasound and Photoacoustic Dual-Modality Imaging".* Ayeeshik Kole[1,2], Yingchun Cao[2], Jie Hui[2], Pu Wang[2], Islam Bolad[1], Ji-Xin Cheng[1,2], Michael Sturek[1,2]; [1] Indiana University School of Medicine, [2] Purdue University |
| **9** | *"Combination of micro CT with infrared spectroscopy provides the most complete approach for stone analysis".* James C. Williams, Jr. and James E. Lingeman; Indiana University School of Medicine |
| **10** | *"Magnetization Transfer MRI Noninvasively Detects Renal Fibrosis Swine Atherosclerotic Renal Artery Stenosis at 3.0 T".* Kai Jiang, Christopher M. Ferguson, John R. Woollard, James D. Krier, and Lilach O. Lerman; Mayo Clinic, Rochester, MN |
| **11** | *"Magnetic Resonance Diffusion Tensor and q-space imaging in an Animal Model of Chronic Kidney Disease".* Sourajit M. Mustafi,Paul R. Territo, Brian P. McCarthy, Amanda A. Riley, Jiang Lei, Chen Lin, Qiuting Wen, Bruce A. Molitoris, Gary D. Hutchins, and Yu-Chien Wu: Indiana University School of Medicine |
| **12** | *"Development of a Novel Magnetic Resonance Imaging (MRI) Acquisition and Analysis Workflow for the Quantification of Renal Hemorrhagic Injury".* Paul R. Territo, Rajash K. Handa, Philip M. Blomgren, Lin Chen, Cynthia D. Johnson, Lie Jiang, Bret A. Connors and Gary D. Hutchins; Indiana University School of Medicine |
| **13** | *"Volumetric Comparison of Automatically Segmented Hippocampal Subfields from 4-Min Accelerated versus 8-Min T2-weighted 3T MRI Scans".* Shan Cong, Shannon L. Risacher, John D. West, Yu-Chien Wu, Liana Apostolova, Eileen Tallman, Maher Rizkalla, Paul Salama, Andrew J. Saykin, Li Shen; Indiana University Purdue University Indianapolis & Indiana University School of Medicine |
| **14** | *"Physics of Drug Transport".* Meysam Tavakoli[1], Konstantinos Tsekouras[1], Richard Day[2], Ken Dunn[2], and Steve Pressé[1]; [1]Indiana University-Purdue University, Indianapolis; [2]Indiana University School of Medicine. |
| **15** | *"The Growth and Impact of ADNI Genetics Publications as Measured by Science Mapping".* Xiaohui Yao[1,2], Jingwen Yan[1,2], Michael Ginda[3], Katy Borner[3], Sungeun Kim[1,8], Kwangsik Nho[1], Shannon L. Risacher[1], Tatiana M. Foroud[1], Steven G. Potkin[4], Paul M. Thompson[5], Jason H. Moore[6], Michael W. Weiner[7], Andrew J. Saykin[1], Li Shen[1,2], for the Alzheimer's Disease Neuroimaging Initiative (ADNI); [1]IU School of Medicine; [2]IU School of Informatics and Computing; [3]IU School of Informatics and Computing, Bloomington, IN; [4]University of California, Irvine, CA; [5]USC Keck School of Medicine, Los Angeles, CA; [6]School of Medicine, University of Pennsylvania, Philadelphia, PA; [7]UCSF School of Medicine, San Francisco, CA, USA; [8]Department of Electrical and Computer Engineering, Oswego, NY |

# Indiana Consortium for Innovation in Biomedical Imaging

Gary D. Hutchins and Mark R. Holland

*Indiana University-Purdue University Indianapolis & Indiana University School of Medicine*

The **Indiana Consortium for Innovation in Biomedical Imaging (Indiana-CIBI)** has been established to leverage the biomedical imaging strengths of several major academic institutions throughout Indiana. This initiative provides the environment, infrastructure, and resources necessary for establishing one of the premier translational, research and educational imaging networks in the United States. The Indiana-CIBI will facilitate the identification of crucial clinical problems and unmet research needs; stimulate the development of innovative solutions; and help translate optimized patient care services into practice at partner health-care delivery facilities.

The **objectives** of the *Indiana-CIBI* include:

- *Providing national leadership in translation from concept to practice.*
- *Encouraging targeted problem-driven technology development.*
- *Nurturing innovation and progress through facile access to advanced resources.*
- *Focusing Indiana state-wide interdisciplinary partnerships in the development of new, innovative imaging technologies and the utilization of imaging resources.*
- *Cultivating investigator engagement and channeling intrinsic motivation.*

The stated objectives of the Indiana-CIBI define the operational model for the consortium. Key steps in the innovation-focused process include: 1) Identification of critical clinical or biomedical research needs by physician or biomedical investigator(s); 2) Creation of innovative solutions through innovation incubator teams, imaging innovation marathons, and crowdsourcing solicitations; 3) Translation to practice through a large medical physics/radiology network; and 4) Translation to advanced core services through the Indiana-CTSI core resource network. Critical success factors for the Indiana-CIBI include tight integration within academic health care facilities, consolidation of fragmented resources, and expansion of critical support resources, eliminating the need to duplicate some types of services across multiple sites in Indiana.

*For further information regarding the Indiana Consortium for Innovation in Biomedical Imaging and its programs please contact Mark Holland or Gary Hutchins at incibi@iupui.edu. The Indiana-CIBI is supported, in part, by contributions from the IUPUI Office of the Vice Chancellor for Research.*

# Research Center for Quantitative Renal Imaging

Bruce A. Molitoris, Gary D. Hutchins, and Mark R. Holland

*Indiana University-Purdue University Indianapolis & Indiana University School of Medicine*

***Mission:*** The overall mission of the *Research Center for Quantitative Renal Imaging* is to provide a focused research environment and resource for the development, implementation, and dissemination of innovative, quantitative imaging methods designed to assess the status of and mechanisms associated with acute and chronic kidney disease and evaluate efficacy of therapeutic interventions.

***Nature of the Center:*** IUPUI has several established research programs focused on understanding the fundamental mechanisms associated with kidney diseases along with established groups of investigators dedicated to the development of advanced imaging methods and quantitative analyses. This Research Center provides a formal mechanism to link these independently successful research efforts into a focused effort dedicated toward the development and implementation of quantitative renal imaging methods.

The **goals** of the *IUPUI Research Center for Quantitative Renal Imaging* are to:

- Identify, develop, and implement innovative imaging methods that provide quantitative imaging biomarkers for assessing and inter-relating renal structure, function, hemodynamics and underlying tissue micro-environmental factors contributing to kidney disease.
- Establish an environment that facilitates and encourages interdisciplinary collaborations among investigators and offers research support to investigators focused on developing and utilizing innovative quantitative imaging methods in support of kidney disease research.
- Provide a resource to inform the greater research and healthcare communities of advances in quantitative renal imaging and its potential for enhanced patient management and care.
- Offer an imaging research resource to companies engaged in product development associated with the diagnosis and treatment of kidney diseases.

***Further Information:*** For further information regarding the *IUPUI Research Center for Quantitative Renal Imaging* and its funding programs please visit http://www.renalimaging.iupui.edu/ or contact the Center at renalimg@iupui.edu.

***Acknowledgments:*** The *IUPUI Research Center for Quantitative Renal Imaging* is supported by contributions from the IUPUI Signature Center Initiative, the Department of Radiology & Imaging Sciences; the Division of Nephrology, the IUPUI School of Science, the IUPUI School of Engineering & Technology, and the Indiana Clinical and Translational Sciences Institute (CTSI).

**“Indiana Center for Biological Microscopy”**

Kenneth Dunn, Malgorzata Kamocka, Seth Winfree, Bruce Molitoris

The Indiana Center for Biological Microscopy “ICBM” has been providing imaging capabilities to Indiana University Researchers since 1996. In 2002 the ICBM has become the NIDDK George O'Brien Center for Advanced Microscopic Analysis, whose objective is to develop methods of intravital multiphoton microscopy for renal research. For the last few years the Center has been providing an intravital microscopy service for Cancer Center investigators through the Optical Microscopy Core for the CEMH.

We are organized around the principle of providing researchers with access to and training on the latest instruments in optical microscopy. We emphasize hands-on access to instruments for individual investigators and unparalleled assistance from on-staff imaging experts. In addition to providing efficient, state-of-the-art biomedical imaging support, the center is also actively involved in biological imaging research and the development of new methods of microscopy and digital image analysis software.

The ICBM imaging facility is located in Research II Building (second floor) of IUPUI campus and is available to anyone at the Indiana University and researchers from outside the institution.

# The 3D Bioprinting Core at IUSM/IUPUI

L. J. Smith, PhD* and N. I. Moldovan, PhD**

*Department of Radiology and Imaging Sciences, I. U. School of Medicine, Indianapolis, Indiana

**Department of Ophthalmology, Indiana University-Purdue University at Indianapolis, Indianapolis, Indiana

Prenatal and post-natal development, wound healing, and other tissue generating activities in the body rely on processes whereby aggregates of cells generate tissues. During this process, cell aggregates rely on cues form cell-cell contact, other internal cues, and external cues to stimulate extracellular matrix secretion, cell migration (self-organization) within the aggregate, and cellular differentiation, thereby resulting in a tissue.

Ideally, engineering a tissue construct should be achieved in a similar process. While small cell aggregates called spheroids (1,000 to 100,000 cells each) have been studied, assembling spheroids into larger cell aggregates into a useful tissue construct was only achieved with the recent launch of the semi-automated ‘Regenova’ 3D-bioprinter. Using robotically-controlled placement, the Regenova assembles (prints) cell spheroids into a pre-designed 3D pattern onto a temporary support made from an array of microneedles. The spheroids remain on the needle support as the spheroids fuse to one another. Meanwhile, cells within the spheroids react to internal and external cues promoting extracellular matrix production, cell migration, and differentiation, forming a tissue construct

Renal imaging related 3D bioprinting applications include generating healthy and damaged tissue models for imaging analysis, characterizing tissue response to imaging reagents, and developing tissue-based precision medicine models.

Peer-reviewed publications demonstrate that this tissue engineering approach is viable for bioprinting vascular, tracheal, and urethral tubes, and other tissue constructs. The first Regenova for academic use in North America was installed on the IUSM/IUPUI campus and is the featured instrument in the newly formed 3D Bioprinting Core. Our Core facility is staffed with qualified personnel to support bioprinting projects. We have begun working with labs on projects addressing bone, cartilage, liver, pancreas, skin, vasculature, etc. This facility will initiate significant tissue engineering and biofabrication progress at IUSM/IUPUI, placing our institution and its medical school at the forefront of the biofabrication revolution.

# Image-based Computational Assessment for Severity of Renal Artery Stenosis

Huidan (Whitney) Yu[a,b], Anurag Deb[a], Avinash Mumbaraddi[a], Alan P. Sawchuk[b], Raghunandan Motaganahalli[b], Michael C. Dalsing[b]

[a]Mechanical Engineering Department, Indiana University-Purdue University, Indianapolis (IUPUI), Indiana 46202, USA

[b]Division of Vascular Surgery, School of Medicine, Indiana University, Indiana, 46202, USA

We develop a computational technique of modeling and analysis based on patient's CT/MRI imaging information and Doppler Ultrasound test for non-invasive assessment of the severity of renal artery stenosis (RAS) through its contribution to the overall renal resistance. The attractive advantages of such a technique include the low cost of facility, personnel, and supplies; the fully human subject protection; the short and flexible time cycle, and the direct human subject results. Unified mesoscale lattice Boltzmann models, for anatomical extraction and fluid dynamics, and GPU (Graphics Processing Unit) parallel computing technology are seamlessly integrated in one computational platform thus neither data transformation and mesh generation nor remote supercomputing required to achieve fast computation within clinically accepted time for medical diagnose and assessment. We establish the relationship between the degree of stenosis (S), and the physical attributes related to the renal resistance through a parametric study by varying S. Our computational results include three aspects. First, pressure decreases across a stenosis. When S increases, the transstenotic pressure gradient increases and the flow rate decreases. Second, the contribution of a RAS to the total renal resistance is minor and changes slowly when S < 85% whereas it becomes significant and changes rapidly when S > 85%. Third, it is found that the renal resistive index (RRI) remains almost the same when S < 73%. It decrease rapidly when S > 73%. Our computational study suggests that renal artery stenting would only benefit patients with large degree of stenosis, i.e. 85%, and that the current clinically utilized RRI may not be an appropriate indicator for renal resistance. However, more application applied studies and corresponding validation with invasive medical measurements medical validations are required before a definitive conclusion can be made.

# The Complex Hemodynamics in Aortorenal Vessel System

AP Sawchuk[a], W. Yu[a,b], MC Dalsing[a]
[a]Division of Vascular Surgery, School of Medicine, Indiana University, Indiana, 46202
[b]Mechanical Engineering Department, Indiana University-Purdue University, Indianapolis (IUPUI), Indiana 46202

This study evaluates the interrelationship between the renal artery anatomy, intrinsic resistance and shear stress in order to understand the forces leading to renal artery atherosclerosis. Patient specific computational modeling of renal artery blood flow derived from CT arteriography was used to evaluate the relationship between renal artery anatomy, intrinsic renal arteriolar resistance, shear stress and plaque formation. The fluid dynamic techniques used have been validated with patient specific duplex ultrasound results and experimental studies done in our laboratory and others. The anatomy of the aorta and renal arteries had the greatest effect on vorticity and shear stress and our findings of eddy currents and areas of low shear on the cephalad wall of the renal artery correlated with a previous experimental finding of plaque development primarily occurring in this region. Beyond anatomical effects, small changes (25 percent) in distal intrinsic renovascular resistance consistent with increased arteriolar tone had a significant effect on further flow and pressure distortions and shear stress reductions. The presence of up to 40 percent renal artery stenosis at the orifice had little effect on these parameters.The anatomic relationship of the aorta and renal arteries as well as small changes (25 percent) in renal arteriolar tone have significant effects on renal artery blood flow patterns, pressures and shear stress which potentiate the development of atherosclerosis. Up to 40 percent renal artery stenosis at the orifice had little effect. These limited changes in intrinsic renovascular resistance are the one factor that is most treatable for the prevention of renal artery stenosis. This level of resistance may be below the level detectable by the renal resistance index. Improved methods for detecting small changes in renovascular resistance and medications or treatments specifically modifying end arteriole tone are needed to limit the morbidity and mortality of renovascular disease.

**IUPUI Imaging Research Symposium – Advances in Renal Imaging**

# High Frequency Ultrasound of *In Vivo* Murine Renal Artery and Vein Blood Flow

Frederick Damen[1], Arvin Soepriatna[1], Shelby Abrams[1], Amy Bogucki[1], Ron Korstanje[2], Craig J. Goergen[1]
[1]Purdue University, West Lafayette, IN; [2]The Jackson Laboratory, Bar Harbor, ME

The renal system serves a critical role in the modulation of plasma composition and volume, maintaining body fluids in homeostatic conditions. In order to further our understanding of how blood flow to the kidneys is affected by glomeruli density, we used high frequency ultrasound to measure renal blood flow of both C57BL/6J (B6) and FVB/J (FVB) mice *in vivo*. We hypothesized that B6 mice, previously shown to have a larger glomeruli count, will have higher arterial and venous blood flows. Two-dimensional B-Mode, M-Mode, color Doppler, and pulsed wave Doppler were acquired using a 40MHz transducer on two separate occasions for both left and right renal arteries and veins (n=8 B6, n=8 FVB). Mean arterial blood flow was higher in B6 mice when compared to FVB mice for both right (52.5±22.3 $mm^3/s$ vs. 26.6±13.2 $mm^3/s$, $p<0.05$) and left (47.4±18.6 $mm^3/s$ vs. 31.7±21.5 $mm^3/s$, $p<0.05$) kidneys. Mean venous blood flow was also higher between B6 and FVB mice in both right (34.7±13.7 $mm^3/s$ vs. 18.6±8.8 $mm^3/s$, $p<0.05$) and left (32.4±11.2 $mm^3/s$ vs. 15.0±10.7 $mm^3/s$, $p<0.05$) kidneys. Figure 1A shows the outline of a kidney overlaid onto a sample color Doppler image. Figure 1B shows an example of both arterial and venous pulsed wave Doppler analyses for that same kidney. In conjunction with our original hypothesis, B6 mice showed higher measured arterial and venous blood flows, potentially due in part to the higher number of glomeruli. Future work will focus on imaging other murine strains with varying glomeruli densities.

**Figure 1**

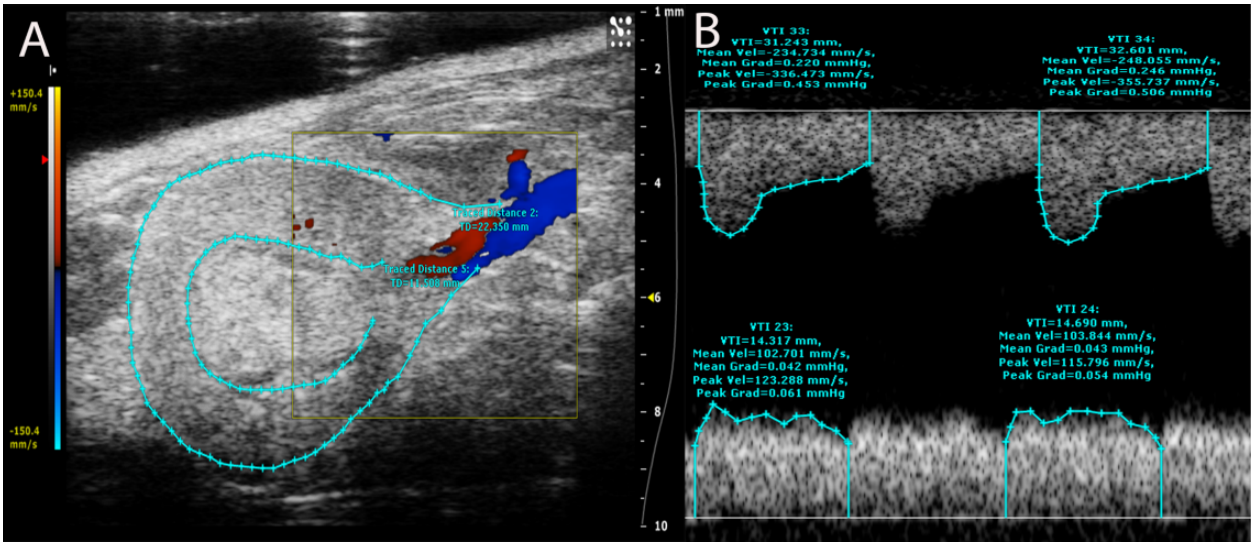

1

**Combination of micro CT with infrared spectroscopy provides the most complete approach for stone analysis**

*James C. Williams, Jr.*, James E. Lingeman, Indianapolis, IN*

INTRODUCTION AND OBJECTIVES: Analysis of composition of urinary stones is essential for proper diagnosis and management, but existing methods are known to be prone to error and are difficult to assess for accuracy using real stone specimens. Our group has been using micro CT for stone analysis now for 15 years, and here we report our results for analyses with patient stone specimens.

METHODS: All stones were macro-photographed and then scanned using a Skyscan 1172 Micro CT system, a non-destructive method. Following this, stones were analyzed using a Bruker Alpha-T Infrared Spectrometer (FT-IR), and results were compared.

RESULTS: In 472 stone specimens, the majority minerals were calcium oxalate (CaOx, 60.0%), apatite (12.3%), struvite (8.5%), uric acid (8.1%), brushite (7.6%), and minor types (3.6%) that included cystine, urates, various phosphates, and pharmaceuticals. Micro CT by itself correctly identified all the major and minor minerals in 86.4% of the specimens. About half of the failures with micro CT were for rare components (e.g., whitlockite), but micro CT also missed brushite in 11 of the 36 specimens containing that mineral, as brushite can appear on micro CT with an x-ray attenuation value very close to that of CaOx. There were also 14 specimens in which micro CT either failed to detect or incorrectly specified struvite; this is because struvite often mixes with other minerals in a manner that makes it difficult to recognize. FT-IR was also found to be in error in 12.5% of the specimens because it missed minor components (typically apatite in low total percentage in the specimen) that were confidently identified using micro CT. Used together, the combination of micro CT with FT-IR provides what is arguably the most complete analysis of urinary stones that is presently available. Moreover, the combination allows identification of complex mineral combinations within stones, as the micro CT imaging can target specific regions of a specimen for FT-IR analysis (see figure).

CONCLUSIONS: Accurate identification of stone mineral is a difficult challenge beyond the ability of a single methodology. The non-destructive nature of micro CT makes it a powerful complement to existing spectroscopic methods for analyzing stones.

**Source of Funding:** NIH P01 DK56788, NIH S10 RR023710

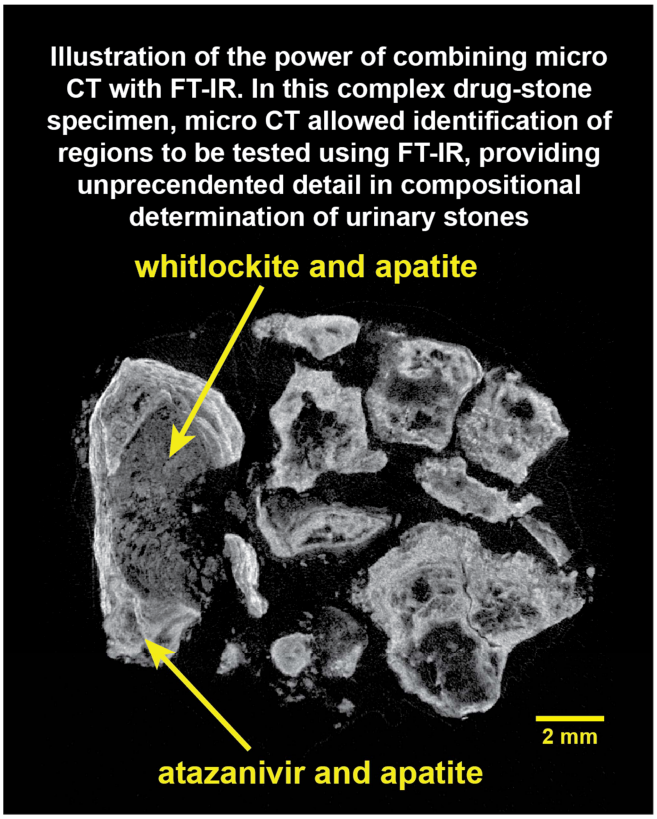

# Magnetization Transfer MRI Noninvasively Detects Renal Fibrosis Swine Atherosclerotic Renal Artery Stenosis at 3.0 T

Kai Jiang[1], Christopher M. Ferguson[1], John R. Woollard[1], James D. Krier[1], and Lilach O. Lerman[1]

[1]*Division of Nephrology and Hypertension, Mayo Clinic, Rochester, Minnesota, USA*

## Introduction

We have previously shown that magnetization transfer (MT)-MRI, which evaluates the presence of macromolecules, offers a noninvasive tool to probe renal fibrosis in murine renal artery stenosis (RAS) at 16.4 T. We hypothesized that MT-MRI can detect renal fibrosis in a swine model of atherosclerotic RAS (ARAS) at 3.0 T.

## Methods

**Phantom Study.** MRI studies were performed on a GE Signa HDxt 3.0 T scanner using an MT-prepared gradient echo sequence. The appropriate offset frequency was selected in a collagen phantom study. Images with ($M_t$) and without ($M_o$) MT preparation were acquired and MT ratio (MTR) calculated as: $(M_0-M_t)/M_0$. The percentage change in MTR (%chMTR) compared to a reference frequency was also calculated.

**Animal Study.** Ten weeks after RAS induction in 6 control and 7 ARAS pigs, cortical and medullary MTRs were measured and normalized by dorsal muscle MTR to correct for $B_1$ variation. The %chMTR from 1000 to 600 Hz was then calculated.

Masson's trichrome staining was subsequently performed on harvested kidney and the fraction of tissue fibrosis quantified.

## Results

**Phantom Study** The 50% collagen phantom showed larger MTRs (Fig. 1a&b) but smaller %ch MTRs (Fig. 1c) than 25% collagen. To achieve high MT sensitivity with little free water saturation, offset frequencies at 600 and 1000 Hz were chosen for *in-vivo* studies.

**Animal Study.** Greater MTR in ARAS vs. normal kidneys (Fig. 2a) was more evident at 1000 than 600 Hz (Fig. 2b), whereas %chMTR was markedly lower in ARAS kidneys (Fig. 2c).

ARAS kidneys showed more fibrosis than controls (Fig. 2d-e). Compared to MTR (Fig. 3a&b), %chMTR (Fig. 3c&d) showed a better correlation with *ex-vivo* fibrosis.

## Conclusion

A change in renal MTR values between offset frequencies may be a novel and useful tool for detecting renal fibrosis in swine ARAS at 3.0 T MRI.

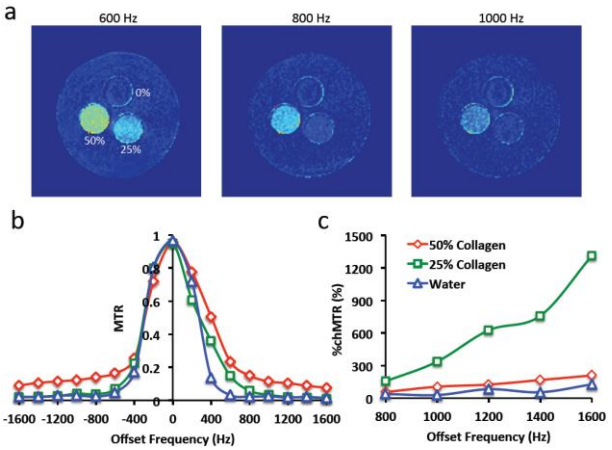


**Figure 1. Phantom study. a**. Representative MTR maps at 600, 800, and 1000 Hz. **b**. MTR with offset frequency from -1600 to 1600 Hz. **c**. %chMTR at different offset frequencies (800 to 1600 Hz) with the reference frequency at 600 Hz.

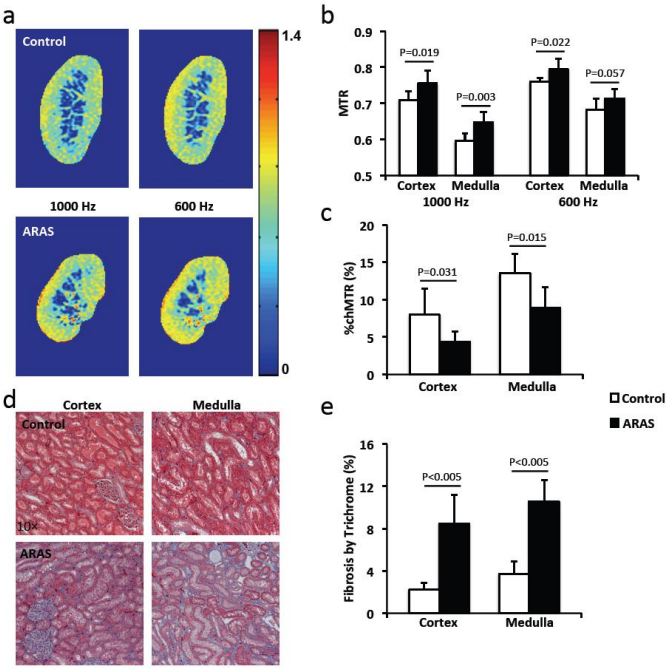


**Figure 2. *In-vivo* MT. a**. Representative MTR maps of control and ARAS kidneys at 1000 and 600 Hz. **b**. Cortical and medullary MTR. **c**. Cortical and medullary %chMTR. **d**. Representative images of trichrome-stained cortical and medullary tissues from control and ARAS kidneys. **e**. Degree of fibrosis quantified from trichrome staining.

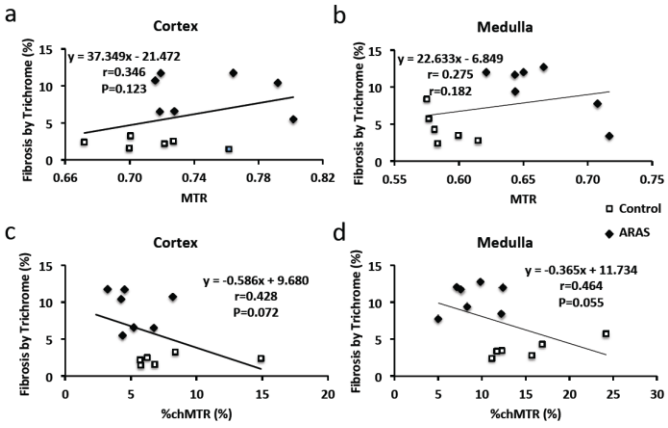


**Figure 3.** Correlation between fibrosis by *ex-vivo* trichrome staining and *in-vivo* MTR at 1000 Hz (**a**&**b**) or %chMTR (**c**&**d**) in cortex (**a**&**c**) and medulla (**b**&**d**).

**Title**

Magnetic Resonance Diffusion Tensor and q-space imaging in an Animal Model of Chronic Kidney Disease.

**Authors**

Sourajit M. Mustafi[1],Paul R. Territo[1], Brian P. McCarthy[1], Amanda A. Riley[1], Jiang Lei[1], Chen Lin[1], Qiuting Wen[1] Bruce A. Molitoris[2], Gary D. Hutchins[1], and Yu-Chien Wu[1]

**Synopsis (limit 100 words)**

In this study, we used multi-shell diffusion-weighted imaging in an animal model of Chronic Kidney Disease (CKD). We focus on the functional changes in the kidney using diffusion tensor imaging (DTI) and q-space imaging (QSI). Four Wistar rats received surgical procedure to induce ischemic fibrosis in their left kidney. The multi-shell diffusion-weighted imaging was performed on the acute stage, day 2 after the surgery. In the acute stage, the renal medulla showed significant decrease in overall diffusivity measured by DTI and increase in tissue restriction measured by q-space imaging.

Words: 89

**Limit 750**

**Purpose:**

Chronic Kidney Disease (CKD) is characterized by progressive renal fibrosis that leads to end-stage renal failure and the need for dialysis or kidney transplantation[1]. There is a compelling need for the development of biomarkers to monitor CKD progression and help guide the evaluation of experimental treatment strategies. We hypothesize that characteristics of water diffusion and flow will serve as a biomarker for renal fibrotic burden. The objective of this study is to develop and evaluate the utility of magnetic resonance imaging based diffusion tensor[2] and non-parametric q-space imaging techniques[3] as biomarkers of renal fibrosis in an animal model of CKD.

**Method:**

***Preparation of the animal CKD model:*** An ischemia/reperfusion model was used to create hypoxia induced renal fibrosis in Wistar rats (N=4). In each animal the renal artery in one kidney was clamped for 50 minutes to induce ischemia and hypoxia (IHK), followed by restoration of blood flow. The contralateral kidney served as a control reference (CON). ***MRI imaging:*** MRI was performed 2 days following surgery. During each imaging session, rats were sedated and placed in a head-first prone position. All animal handling followed institutional Animal Care and Use Committee (IACUC) guidelines. The MRI diffusion pulse sequence was a single-shot spin-echo echo-planar imaging (SS-SE-EPI) sequence with multiple diffusion-weighting b-values (i.e. 3 shells with b-values of 150, 300 and 450 s/mm$^2$) and multiple diffusion-weighting directions at each shell (i.e., 10, 19 and 30, respectively). Diffusion directions in each shell and in the projected sphere with all directions (i.e., total 59) were optimized for uniform diffusion sampling in the spherical space[4]. The repetition time (TR) is 2200 ms and echo time (TE) is 73.6 ms. A total of four signal averages was performed. The imaging parameters were field-of-view (FOV) = 128 x 64 mm, matrix size = 128 x 64, isotropic voxel size of 1 mm$^3$, and 20 oblique coronal slices. ***Image Processing:*** DTI derived parameters including axial diffusivity (AD), radial diffusivity (RD), mean diffusivity (MD), and fractional anisotropy (FA) were computed[5]. A non-parametric q-space approach was used to compute the probability density function (PDF), a marker of very slow water diffusion ($P_0$)[3]. ***ROIs***: In the $b_0$ image, anatomically defined layers of kidney are clearly identified. Two distinct ROIs were placed on medulla and cortex (Figure 1). ***Statistics:*** Student's paired two tailed t-test were performed on individual ROI's and multiple comparison Bonferroni corrections were implemented, two-tail p value < 0.01 was considered significant.

## Results

All DTI indices (AD, RD, MD, and FA) showed statistically significant reductions in the medulla of the IHK kidneys (Figure 2A and B). The tissue restriction index, $P_0$, increased in the medulla of the IHK kidneys ($p < 0.01$). No significant changes in DTI parameters or tissue restriction index were observed in the renal cortex of the IHK kidneys (Figures 2C and D).

## Discussion and Conclusion

The observed reduction in mean diffusivity measured with DTI and increased $P_0$ (population of very slowly diffusing water molecules) in renal medulla are consistent with the formation of fibrotic regions within the tissue. It is thought that DTI axial diffusivity is an indicator of intra-tubular flow in the renal medulla[6-9] and radial diffusivity is an indicator of water reabsorption rate[6]. The changes in AD and RD observed in this study suggest that intra-tubular flow and water reabsorption rate decreased in the IHK kidney. The dramatic decrease in FA suggests the impact of intra-tubular flow is much higher that the impact of water reabsorption rate in our renal hypoxia induced fibrosis model. In addition, the medulla appear more sensitive ischemia induced hypoxia than renal cortices.

Words: 587


## Acknowledgment

The work is supported by IUPUI-RITDP pilot grant.


## References:


1. Tonella M, Riella M. Chronic Kidney Disease and the Aging Population. Nephrol Dial Transplant 2014;29(2):221-224.
2. Wang WJ, Pui MH, Guo Y, Wang LQ, Wang HJ and Liu M. 3T magnetic resonance diffusion tensor imaging in chronic kidney disease. Abdom Imaging. 2014 Aug; 39(4): 770-775.
3. Wu YC, Alexander AL. Hybrid diffusion imaging. Neuroimage. 2007;36(3):617-29. PMCID: 2428345.
4. Caruyer E, Lenglet C, Saprio G, and Deriche R. Design of multishell sampling schemes with uniform coverage in diffusion MRI. Magnetic Resonance in Medicine 2013;69:(6)1534-1540.
5. Basser PJ, LeBihan MJ. Estimation of the effective self-diffusion tensor from the NMR spin echo Magn Reson B 1994;103(3):247-54.
6. Sigmund EE, Vivier PH, Sui D, et al. Intravoxel incoherent motion and diffusion-tensor imaging in renal tissue under hydration and furosemide flow challenges. Radiology. 2012;263(3):758-69
7. Liu, Z. *et al.* Chronic kidney disease: pathological and functional assessment with diffusion tensor imaging at 3T MR. *European radiology* **25**, 652-660, doi:10.1007/s00330-014-3461-x (2015).

8. Hueper K, Hartung D, Gutberlet M, Gueler F, Sann H, Husen B, Wacker F, Reiche D. Magnetic resonance diffusion tensor imaging for evaluation of histopathological changes in a rat model of diabetic nephropathy. Invest Radiol. 2012;47(7):430-7.

9. Wang WJ, Pui MH, Guo Y, Wang LQ, Wang HJ, Liu M. 3T magnetic resonance diffusion tensor imaging in chronic kidney disease. Abdominal imaging. 2014;39(4):770-5.

**Figure Caption limit 50 words**

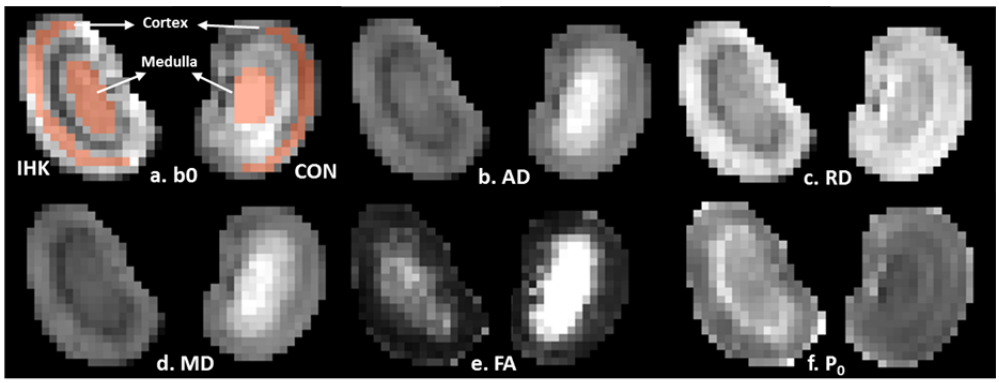


Figure 1: b0 (with ROIs), DTI and P0 maps for CON and IHK kidney after two days of surgical intervention. The scale of AD, RD and MD are from 0 to 3, 1.5 and 3*10$^{-3}$ mm$^2$/s respectively. FA and Po are scaled from 0 to 0.4 and 0.3 to 0.8 respectively.

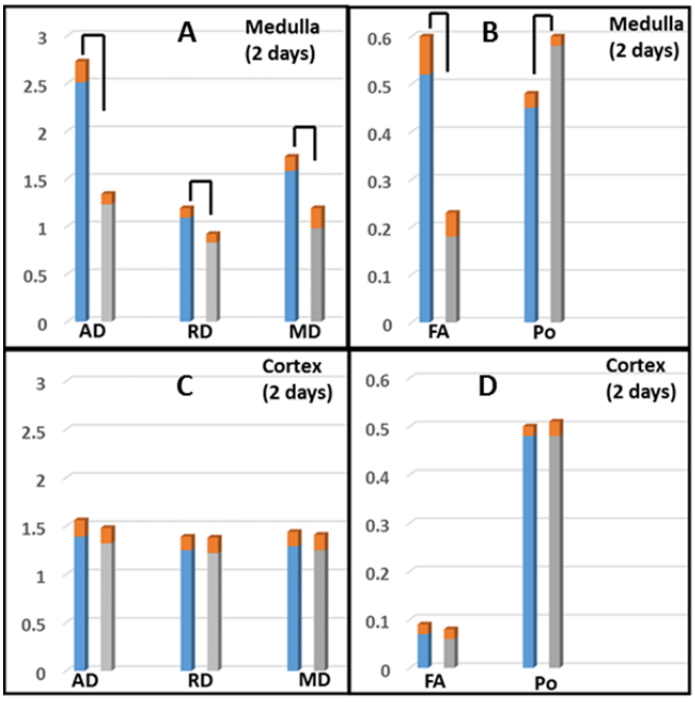


Figure 2: DTI and q-space parameters for various ROIs are compared between CON (blue bars) and IHK (grey bars) kidney. The orange bars denotes standard deviations. The statistically significant parameters ($p < 0.01$) are shown by connecting lines. The units for diffusivity are 1*10$^{-3}$ mm$^2$/s..

# Development of a Novel Magnetic Resonance Imaging (MRI) Acquisition and Analysis Workflow for the Quantification of Renal Hemorrhagic Injury.

Paul R. Territo[1], Rajash K. Handa[2]*, Philip M. Blomgren[2], Lin Chen[1], Cynthia D. Johnson[2], Lie Jiang[1], Bret A. Connors[2] and Gary D. Hutchins[1].

[1]Department of Radiology and [2]Department of Anatomy and Cell Biology, Indiana University School of Medicine

**Introduction and Objective.** Shock wave lithotripsy (SWL) has been used as an effective noninvasive treatment for nephrolithiasis; however, SWL can produce undesirable side effects in the target tissue resulting in renal hemorrhagic injury. The current gold standard for quantifying SWL-induced tissue damage is based on morphometric detection of renal hemorrhage in serial tissue sections from fixed kidneys. This methodology is time/labor intensive; requires expert knowledge of renal anatomy and image processing to generate accurate results and is tissue destructive. We sought to develop a non-destructive method that would permit rapid assessment of whole kidney hemorrhagic lesions in post-mortem organs using native tissue contrast that would reduce cycle time while maintaining information content of lesion volumes.

**Methods.** Kidneys of anesthetized adult farm pigs were targeted with shock waves (SWs) using the Compact S lithotripter (2500 SWs at various power levels and SW rates). Kidneys were then perfusion fixed *in situ*, harvested and prepared for tissue injury quantification. T1 weighted (T1W) 3D-FLASH and T2 weighted (T2W) 3D-SPACE images were acquired on a Siemens 3T Tim Trio using a high sensitivity 72mm inner diameter 8 channel volume coil. Images were co-registered, normalized, difference images generated, and volumes classified and segmented using a Multispectral Neural Network classifier. Kidneys were then subjected to standard morphometric analysis for measurement of lesion volumes.

**Results.** Classifications of T1W, T2W and difference image volumes were correlated with morphometric measurements of whole organ lesion volumes. The data can be described by the relationship $y = 0.49x + 0.03$ ($R^2 = 0.99$, $N = 9$), where the lesions ranged broadly for morphology ($x = 0 - 2.5\%$) and MRI ($y = 0 - 1.3\%$).

**Conclusions.** These preliminary data suggest that the MRI technique may provide a rapid, low cost and reliable means to evaluate renal injury lesion volumes due to SWL and other endourological treatment modalities; and when adapted for in vivo use may provide clinically useful information on the lesion severity, extent, and distribution.

# Volumetric Comparison of Automatically Segmented Hippocampal Subfields from 4-Min Accelerated versus 8-Min T2-weighted 3T MRI Scans

Shan Cong, Shannon L. Risacher, John D. West, Yu-Chien Wu, Liana Apostolova, Eileen Tallman, Maher Rizkalla, Paul Salama, Andrew J. Saykin, Li Shen[1,*]

[1] Indiana University Purdue University Indianapolis

[2]Indiana University School of Medicine

*Correspondence to shenli@iu.edu

## 1. Background

A high resolution (0.4mm in plane) T2-weighted turbo spin-echo sequence has been studied to enable hippocampal subfield volumetry [1,2]. The standard 8 minute protocol is vulnerable to motion in clinical populations. Acceleration by factor 2 saves scan time and reduces susceptibility to motion but at a cost to signal-to-noise ratio. We compared hippocampal subfield volumes using standard and accelerated protocols.

## 2. Materials & Methods

The sample included 12 cognitively normal control (CN), 9 subjective cognitive decline (SCD), 12 mild cognitive impairment (MCI), and 7 Alzheimer's disease (AD) participants recruited from an ongoing study at the Indiana Alzheimer Disease Center (IADC). The standard 8-minute ADNI protocol and a 4-minute accelerated protocol with GRAPPA (activating generalized autocalibrating partially parallel acquisitions) acceleration factor of 2 were run on a Siemens Prisma 3T MRI. ASHS [1] was used to segment 10 primary labels (Table 1). Intraclass correlation coefficients (ICCs) were computed using SPSS 23 to perform reliability tests between 4-minute and 8-minute scans within and across the 4 groups. Pairwise group analyses were performed, covaried for age, gender and total intracranial volume, to determine whether similar group differences could be observed using 4-minute versus 8-minute data.

**Table 1. Results of the Automatic Segmentation of Hippocampal Subfields (ASHS) software**

| Name | Description |
|---|---|
| **Primary Labels** | |
| CA1 | Cornu Ammonis 1 |
| CA2 | Cornu Ammonis 2 |
| DG | Dentate Gyrus |
| CA3 | Cornu Ammonis 3 |
| MISC | Miscellaneous |
| SUB | Subiculum |
| ERC | Entorhinal Cortex |
| B35 | Brodmann Area 35 |
| B36 | Brodmann Area 36 |
| CS | Collateral Sulcus |
| **Compound Labels** | |
| Whole | Combines all primary labels |
| CA23 | Combines CA2 and CA3 |

## 4. Conclusions

The 4-minute and 8-minute protocols, coupled with ASHS segmentation, yield similar volumetric estimates for hippocampal subfields and differences between groups. The accelerated protocol can provide reliable imaging data for investigation of hippocampal subfield volumetry in SCD/MCI/AD-related MRI studies and may be less vulnerable to motion.

## References

1. Human Brain Mapping (2015) 36:258-287.
2. Neuroimage (2010) 53:1208-1224.

**Acknowledgements:** Supported in part by NIH R01 LM011360, K99 LM011384, U01 AG024904, RC2 AG036535, R01 AG19771, P30 AG10133, and NSF IIS-1117335 at IU. Data used in preparation of this article were obtained from the ADNI database, which was funded by NIH U01 AG024904.

## 3. Results

Table 2 shows the results of the ICC analyses within each group and across all the groups.

Table 3 shows the results for group analyses, including CN vs SCD, CN vs MCI, and CN vs AD.

**Table 2. Results of intraclass correlation analysis (ICC). L and R indicate left and right sides respectively.**

| | All (n=40) | | CN (n=12) | | SCD (n=9) | | MCI (n=12) | | AD (n=7) | |
|---|---|---|---|---|---|---|---|---|---|---|
| | ICC | Sig | ICC | Sig | ICC | Sig | ICC | Sig | ICC | Sig |
| **Primary Labels** | | | | | | | | | | |
| L CA 1 | 0.98 | 0.00 | 0.94 | 0.00 | 0.98 | 0.00 | 0.99 | 0.00 | 0.92 | 0.00 |
| R CA 1 | 0.99 | 0.00 | 0.96 | 0.00 | 0.96 | 0.00 | 0.98 | 0.00 | 0.99 | 0.00 |
| L CA 2 | 0.86 | 0.00 | 0.75 | 0.00 | 0.85 | 0.00 | 0.83 | 0.00 | 0.89 | 0.00 |
| R CA 2 | 0.80 | 0.00 | 0.68 | 0.01 | 0.83 | 0.00 | 0.89 | 0.00 | 0.73 | 0.02 |
| L DG | 0.98 | 0.00 | 0.98 | 0.00 | 0.98 | 0.00 | 0.96 | 0.00 | 0.96 | 0.00 |
| R DG | 0.99 | 0.00 | 0.98 | 0.00 | 0.97 | 0.00 | 0.98 | 0.00 | 0.94 | 0.00 |
| L CA 3 | 0.82 | 0.00 | 0.73 | 0.00 | 0.72 | 0.01 | 0.92 | 0.00 | 0.63 | 0.05 |
| R CA 3 | 0.76 | 0.00 | 0.85 | 0.00 | 0.69 | 0.01 | 0.76 | 0.00 | 0.78 | 0.01 |
| L MISC | 0.94 | 0.00 | 0.90 | 0.00 | 0.93 | 0.00 | 0.99 | 0.00 | 0.89 | 0.00 |
| R MISC | 0.93 | 0.00 | 0.95 | 0.00 | 0.92 | 0.00 | 0.97 | 0.00 | 0.95 | 0.00 |
| L SUB | 0.97 | 0.00 | 0.91 | 0.00 | 0.96 | 0.00 | 0.98 | 0.00 | 0.94 | 0.00 |
| R SUB | 0.98 | 0.00 | 0.96 | 0.00 | 0.97 | 0.00 | 0.98 | 0.00 | 0.97 | 0.00 |
| L ERC | 0.91 | 0.00 | 0.81 | 0.00 | 0.94 | 0.00 | 0.94 | 0.00 | 0.85 | 0.00 |
| R ERC | 0.95 | 0.00 | 0.95 | 0.00 | 0.92 | 0.00 | 0.94 | 0.00 | 0.95 | 0.00 |
| L 35 | 0.93 | 0.00 | 0.94 | 0.00 | 0.94 | 0.00 | 0.92 | 0.00 | 0.97 | 0.00 |
| R 35 | 0.97 | 0.00 | 0.94 | 0.00 | 0.96 | 0.00 | 0.95 | 0.00 | 0.96 | 0.00 |
| L 36 | 0.98 | 0.00 | 0.95 | 0.00 | 0.99 | 0.00 | 0.98 | 0.00 | 0.96 | 0.00 |
| R 36 | 0.99 | 0.00 | 1.00 | 0.00 | 0.98 | 0.00 | 0.97 | 0.00 | 0.99 | 0.00 |
| L CS | 0.94 | 0.00 | 0.94 | 0.00 | 0.88 | 0.00 | 0.94 | 0.00 | 0.99 | 0.00 |
| R CS | 0.98 | 0.00 | 0.98 | 0.00 | 0.99 | 0.00 | 0.99 | 0.00 | 0.96 | 0.00 |
| **Compound Labels** | | | | | | | | | | |
| L Whole | 0.99 | 0.00 | 0.97 | 0.00 | 1.00 | 0.00 | 0.99 | 0.00 | 0.96 | 0.00 |
| R Whole | 0.99 | 0.00 | 0.99 | 0.00 | 0.99 | 0.00 | 0.99 | 0.00 | 0.99 | 0.00 |
| L CA2-3 | 0.95 | 0.00 | 0.78 | 0.00 | 0.77 | 0.00 | 0.91 | 0.00 | 0.70 | 0.03 |
| R CA2-3 | 0.82 | 0.00 | 0.87 | 0.00 | 0.69 | 0.01 | 0.78 | 0.00 | 0.86 | 0.00 |

**Table 3. P value of diagnosis effect on subfield volume covaried for age, gender and ICV. L and R indicate left and right sides respectively. Cells with p<0.05 are highlighted.**

| Subfield | CN vs SCD | | CN vs MCI | | CN vs AD | |
|---|---|---|---|---|---|---|
| | 4 min | 8 min | 4 min | 8 min | 4 min | 8 min |
| **Primary Labels** | | | | | | |
| L CA1 | 0.132 | 0.110 | 0.085 | 0.116 | 0.001 | 0.001 |
| R CA1 | 0.068 | 0.093 | 0.164 | 0.200 | 0.006 | 0.006 |
| L CA2 | 0.083 | 0.489 | 0.123 | 0.185 | 0.081 | 0.023 |
| R CA2 | 0.497 | 0.761 | 0.192 | 0.850 | 0.017 | 0.064 |
| L DG | 0.124 | 0.147 | 0.127 | 0.311 | 0.004 | 0.010 |
| R DG | 0.025 | 0.027 | 0.159 | 0.195 | 0.010 | 0.016 |
| L CA3 | 0.454 | 0.738 | 0.471 | 0.493 | 0.126 | 0.010 |
| R CA3 | 0.923 | 0.314 | 0.787 | 0.831 | 0.307 | 0.562 |
| L MISC | 0.733 | 0.823 | 0.135 | 0.139 | 0.298 | 0.403 |
| R MISC | 0.518 | 0.358 | 0.045 | 0.005 | 0.532 | 0.771 |
| L SUB | 0.103 | 0.165 | 0.099 | 0.070 | 0.009 | 0.015 |
| R SUB | 0.064 | 0.090 | 0.237 | 0.193 | 0.128 | 0.110 |
| L ERC | 0.142 | 0.392 | 0.810 | 0.505 | 0.014 | 0.010 |
| R ERC | 0.103 | 0.101 | 0.376 | 0.881 | 0.039 | 0.105 |
| L B35 | 0.266 | 0.654 | 0.559 | 0.761 | 0.019 | 0.038 |
| R B35 | 0.035 | 0.024 | 0.782 | 0.545 | 0.106 | 0.108 |
| L B36 | 0.928 | 0.875 | 0.197 | 0.139 | 0.033 | 0.021 |
| R B36 | 0.380 | 0.446 | 0.197 | 0.177 | 0.081 | 0.101 |
| L CS | 0.981 | 0.871 | 0.269 | 0.086 | 0.760 | 0.659 |
| R CS | 0.828 | 0.864 | 0.793 | 0.722 | 0.761 | 0.976 |
| **Compound Labels** | | | | | | |
| L Whole | 0.320 | 0.437 | 0.100 | 0.093 | 0.006 | 0.007 |
| R Whole | 0.057 | 0.064 | 0.128 | 0.157 | 0.018 | 0.024 |
| L CA23 | 0.311 | 0.623 | 0.326 | 0.325 | 0.089 | 0.007 |
| R CA23 | 0.842 | 0.322 | 0.629 | 0.820 | 0.188 | 0.389 |

Figure 1 shows an example plot of the ICC analysis across all groups. Significant agreement was observed on most measures. While CA2 and CA3 showed lower ICCs, the combined measure CA2-3 demonstrated higher reliability.

**Figure 1. ICC analysis for all the participants (N=40): Intraclass Correlation Coefficients (ICCs) with 95% confidence interval shown as error bars.**

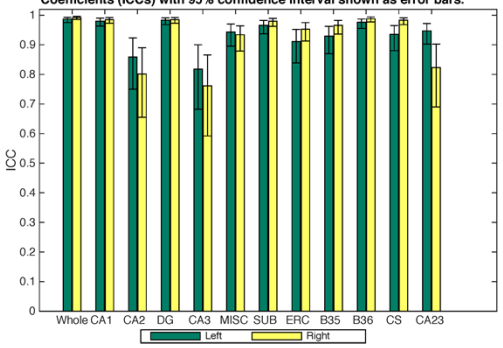


Figure 2 shows two examples of effect size plots. The regional differences detected by the 4-minute data and 8-minute data were very similar.

**Figure 2. Mean and standard error of example measures: (a) CA1, and (b) B35.**

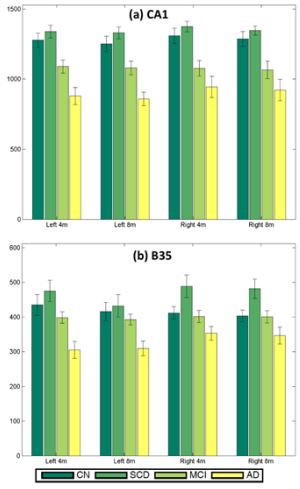

# Physics of Drug Transport

Meysam Tavakoli[1], Konstantinos Tsekouras[1], Richard Day[2], Ken Dunn[3], and Steve Pressé[1]

[1]Physics Department, Indiana Univ.-Purdue Univ. Indianapolis (IUPUI).
[2]Department of Cellular and Integrative Physiology, Indiana Univ., School of Medicine, Indianapolis, Indiana.
[3]Division of Nephrology, Department of Medicine, Indiana Univ., School of Medicine, Indianapolis, Indiana.

**ABSTRACT**

The liver performs a number of critical physiological functions such as processing nutrients and removing toxins from the blood including metabolizing and excreting drugs. For this reason, a major effort in pharmacology is focused on drug liver transport. The goal of this effort is to reduce drug-induced liver injury which is the single biggest source of failure in the development of new drugs and the primary reason for withdrawal of approved drugs from the market. The fundamental process of liver transport is one in which compounds present in the blood are transported into and processed by liver cells.

Here we propose methods to infer the dynamics of transport of fluorescent dyes -- which serve as proxies for drugs -- from data collected in live animals. The proposed study consists of two specific aims: (1) since we expect the fluorescence properties of probes to depend on their location in the living system, we want to determine the relationship between in vivo measured fluorescence and probe concentration, (2) develop a model of molecular transport that would allow us to estimate kinetic parameters not directly measurable.

We have preliminarily proposed a model for liver transport that is defined by a system of non-linear ordinary differential equations.

Our results show that we can develop a novel experimental platform that will extend and fundamentally improve the predictive value of preclinical drug safety studies.

# The Growth and Impact of ADNI Genetics Publications as Measured by Science Mapping

Xiaohui Yao[1,2,*], Jingwen Yan[1,2], Michael Ginda[3], Katy Borner[3], Sungeun Kim[1,8], Kwangsik Nho[1], Shannon L. Risacher[1], Tatiana M. Foroud[1], Steven G. Potkin[4], Paul M. Thompson[5], Jason H. Moore[6], Michael W. Weiner[7], Andrew J. Saykin[1], Li Shen[1,2,*], for the Alzheimer's Disease Neuroimaging Initiative (ADNI)

[1]IU School of Medicine, Indianapolis, IN, USA;
[2]IU School of Informatics and Computing, Indianapolis, IN, USA;
[3]IU School of Informatics and Computing, Bloomington, IN, USA;
[4]University of California, Irvine, CA, USA;
[5]USC Keck School of Medicine, Los Angeles, CA, USA;
[6]School of Medicine, University of Pennsylvania, Philadelphia, PA, USA;
[7]UCSF School of Medicine, San Francisco, CA, USA;
[8]Department of Electrical and Computer Engineering, Oswego, NY, USA
*Correspondence to yao2@umail.iu.edu, shenli@iu.edu

**Background:**

The Genetics Core of the Alzheimer's Disease Neuroimaging Initiative (ADNI) provides genetic resources and facilitate research opportunities in qualitative and quantitative genetics using ADNI multidimensional phenotypes. Genotyping and sequencing data have been generated for ADNI-1/GO/2 participants, and are available to the scientific community. Here we visualize and evaluate the scientific growth and impact of ADNI genetics studies published from 2008 through 2015.

**Methods:**

A Scopus publication search, using keywords related to both ADNI and genetics, was performed to identify papers published between 2008-2015. Manual filtering was used to identify publications where ADNI genetics data were analyzed. Google Refine was applied to unify author names within one institution and keywords. Science of Science Tool (Sci2) [1] was employed to perform a comprehensive evaluation and visualization of institution-level collaborations among ADNI genetics studies, and interactions among ADNI genetics research topics.

**Results:**

The Scopus search followed by manual filtering yielded a total number of 376 ADNI genetics publications. Co-publication networks over this period with statistical evaluation are shown in Figures 1-2. The numbers of institutions and collaborations increased over the years, as did the number of publications. Collaborations jumped in 2014-2015, thanks to both the increased number of publications and several publications with 50+ institutions (e.g., [2]). Figure 3 shows keyword co-occurrence networks at multiple scales: 3,034 links are identified among 428 keywords. Keywords with degree ≥ 5 are labeled and grouped into four categories including genotype, phenotype, analysis and others, where high connections exist among both intra- and inter-category keywords.

**Conclusions:**

Science mapping can reveal the growth and impact of ADNI genetics publications. We observe an increasing number of publications and collaborations, as well as densely interconnected research topics and categories (genotype, phenotype, analysis and others). With the recent release of ADNI multi-omics data (e.g., whole genome sequencing, transcriptomics, and metabolomics), coupled with many other existing and new ADNI resources, we expect to see further growth of ADNI genetics research.

[1] Sci2 Tool. https://sci2.cns.iu.edu.

[2] JAMA Neurology, 71(11): p.1394-1404, 2014.

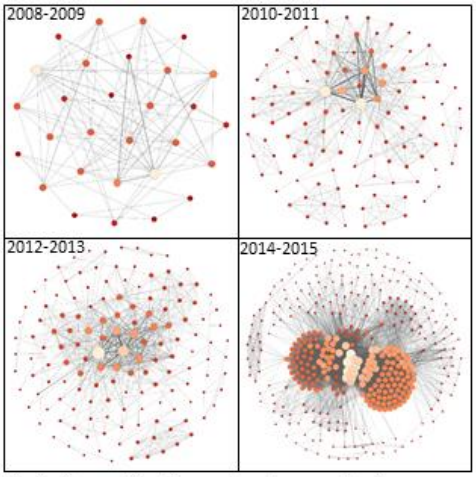


Fig 1. Co-publication networks over the time. Nodes are colored along a color gradient between red (low degree) and white (high degree), and are sized proportional to their degrees.

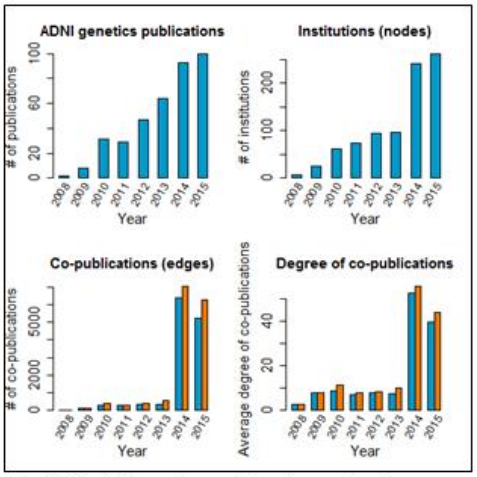


Fig 2. Statistics of co-publication networks. Orange bar indicates total # of institution pairs, and blue bar indicates total # of unique institution pairs, both based on co-publication data.

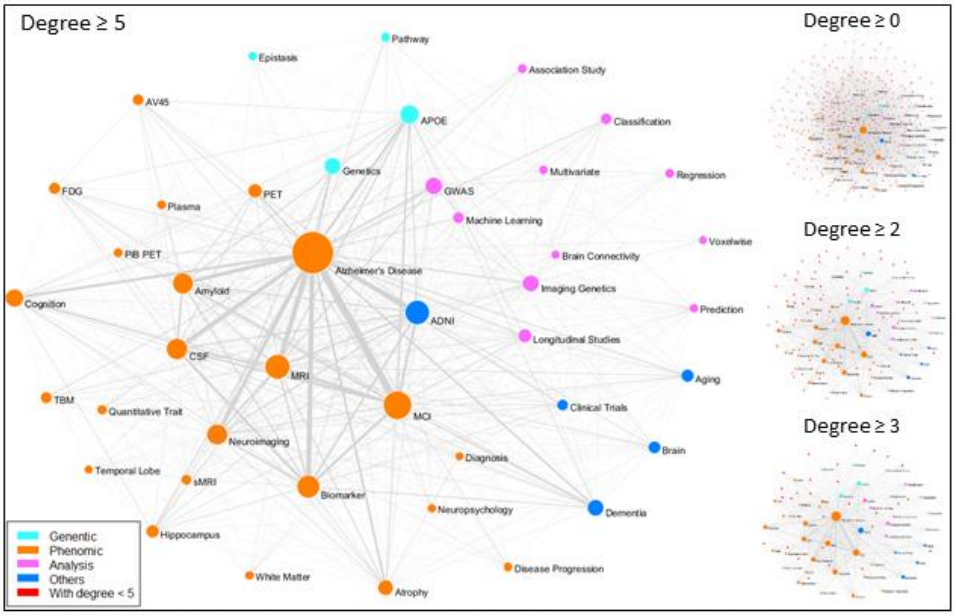


Figure 2. Keyword co-occurrence networks at different scales. Node size proportional to # of papers.